General framework for transport in spin-orbit-coupled superconducting heterostructures: Nonuniform spin-orbit coupling and spin-orbit-active interfaces

Kuei Sun[1,2] and Nayana Shah[1]

[1] *Department of Physics, University of Cincinnati, Cincinnati, Ohio 45221-0011, USA*
[2] *Department of Physics, The University of Texas at Dallas, Richardson, Texas 75080-3021, USA*

Electronic spin-orbit coupling (SOC) is essential for various newly discovered phenomena in condensed-matter systems. In particular, one-dimensional topological heterostructures with SOC have been widely investigated in both theory and experiment for their distinct transport signatures indicating the presence of emergent Majorana fermions. However, a general framework for the SOC-affected transport in superconducting heterostructures, especially with the consideration of interfacial effects, has not been developed even regardless of the topological aspects. We hereby provide one for an effectively one-dimensional superconductor-normal heterostructure with nonuniform magnitude and direction of both Rashba and Dresselhaus SOC as well as a spin-orbit-active interface. We extend the Blonder-Tinkham-Klapwijk treatment to analyze the current-voltage relation and obtain a rich range of transport behaviors. Our work provides a basis for characterizing fundamental physics arising from spin-orbit interactions in heterostructures and its implications for topological systems, spintronic applications, and a whole variety of experimental setups.

PACS numbers: 74.45.+c, 74.25.F-, 71.70.Ej, 74.25.fc

I. INTRODUCTION

The interplay between electronic spin and orbital degrees of freedom, or spin-orbit coupling (SOC), has played a crucial role in various aspects of condensed-matter physics, including the study on semiconductors, ferromagnets, superconductors and materials with exotic orders [1–14] as well as the application on building quantum electronic or spintronic devices [15, 16]. Due to the ubiquity of SOC and superconductivity, it is of fundamental and technological interest to understand their interplay, in particular, in the context of superconducting heterostructures. Furthermore, great interest has been stimulated recently in exploring topological states of matter [17, 18], whose experimental realization and detection strongly rely on transport or scanning tunneling microscopy (STM) measurements of artificially engineered heterostructures with SOC. Among them, those with building blocks such as a semiconductor/topological-insulator wire with SOC and conventional superconductor [19–23] (used to induce a proximity gap) or one-dimensional (1D) ferromagnet combined with a bulk superconductors with SOC [24–28] are of particular interest to explore emerging Majorana fermions [29–35]. Most theoretical studies have focused on either effective models or employed SOC as a uniform model parameter [36–47]. However, the set-up of interest usually has only a segment or end point of the 1D element in contact with a (bulk) superconductor due to either the experimental constraints or an explicit interest in studying (topological) heterostructures [23, 40, 48, 49].

In this paper, we develop a framework to study an (effectively) 1D normal- (N-) superconductor (S) setup (see Fig. 1) that is general enough to capture the effects of SOC in a wide range of (emergent) heterostructures. We allow for both Rashba [50] and Dresselhaus [51] SOC with arbitrary relative strengths on each side as well as at the interface (I), which represents the boundary region [52]. Furthermore, we allow the SOC to have a different magnitude as well as direction in N, S, and I regions. Nonuniform SOC is in fact bound to arise for a variety of reasons including difference in the chemical composition, crystallographic direction, or direction of electric field [50, 51] and may be relevant also for practical implementations of topological quantum computing schemes [53, 54]. SOC in the interface can even simply arise due to a lack of "left-right" symmetry [55–57].

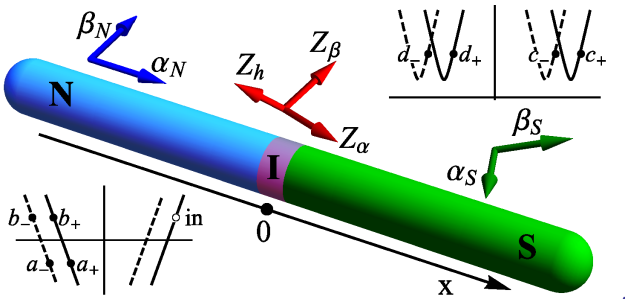

FIG. 1. (Color online) Illustration of an effective 1D N–S system with SOC and a spin-orbit-active interface (I). The vectors denote directions of Rashba $\alpha_{\mathrm{N(S)}}\sigma_y$ and Dresselhaus $\beta_{\mathrm{N(S)}}\sigma_x$ on the N (S) side, as well as interfacial Rashba $Z_\alpha\sigma_y$, Dresselhaus $Z_\alpha\sigma_x$, and Zeeman $Z_h\hat{n}\cdot\vec{\sigma}$ components. In general, the spin basis in each region can be different. Insets: schematic energy spectra with two isospin branches (solid and dashed curves, respectively) on the corresponding sides. The solid circles denote possible outgoing states corresponding to an incoming electron (empty circle) from the N side.

We start by analyzing the appropriate Bogoliubov–de Gennes (BdG) Hamiltonian and develop a generalized Blonder-Tinkham-Klapwijk (BTK) [58] formalism

to calculate the current-voltage characteristics for our general setup. We phenomenologically model what we call the *spin-orbit-active* interface as a generalization of a *spin-active* interface [59–74], which itself is a generalization of a single Z parameter used in the original BTK approach. We find that the rich physics emanating from non-uniform SOC and/or spin-orbit-active interface is not only of fundamental interest but also highly relevent for interpreting the results of experiments. For example, it can effectively lower the interfacial barrier, drastically change the zero-bias conductance, and determine between reentrant or monotonic temperature dependence. Our results also underline the danger in using a single Z-parameter fit to extract the interface properties in experiments as is standard practice. Our analysis offers a more accurate picture even for traditional N-S heterostructures or for STM setups in which a spin-orbit-active interface or the nonzero SOC in the materials may play a role that is not usually taken into account (although the importance of nonzero SOC in the context of pair-breaking effects [75–80] is appreciated).

II. MODEL AND HAMILTONIAN

As illustrated in Fig. 1, our effectively 1D system comprises N ($x<0$) and S ($x>0$) regions with an arbitrary SOC on each side, intersecting at I ($x=0$). The Hamiltonian $H_{j=\mathrm{N,S}}$ in corresponding basis $\Psi_j = \begin{pmatrix} \psi_{\uparrow_j} & \psi_{\downarrow_j} & \psi^\dagger_{\downarrow_j} & -\psi^\dagger_{\uparrow_j} \end{pmatrix}^T$ reads

$$H_{\mathrm{N}} = \tau_z \otimes (E_p \mathbb{1} + \alpha_{\mathrm{N}} p\sigma_y + \beta_{\mathrm{N}} p\sigma_x), \quad (1)$$

$$H_{\mathrm{S}} = \tau_z \otimes (E_p \mathbb{1} + \alpha_{\mathrm{S}} p\sigma_y + \beta_{\mathrm{S}} p\sigma_x) - \Delta\tau_x \otimes \mathbb{1}, \quad (2)$$

where $E_p = \frac{p^2}{2m} - \mu$ is the free spectrum with chemical potential μ, α_j (β_j) are Rashba (Dresselhaus) SOC on the j side, Δ (taken real for convenience) is the s-wave (possibly proximity-induced) superconducting gap, $\vec{\sigma}$ and $\vec{\tau}$ are Pauli matrices spanned in spin and particle-hole basis, respectively, and $\mathbb{1}$ is the 2×2 identity matrix. The spin basis on both sides can differ by an Euler rotation

$$\Psi_{\mathrm{N}} = \left(\mathbb{1} \otimes e^{-i\sigma_z\eta^{(3)}_{\mathrm{NS}}} e^{-i\sigma_y\eta^{(2)}_{\mathrm{NS}}} e^{-i\sigma_z\eta^{(1)}_{\mathrm{NS}}}\right)\Psi_{\mathrm{S}} \equiv U_{\mathrm{NS}}\Psi_{\mathrm{S}}. \quad (3)$$

The two SOCs can be combined as a complex factor

$$\gamma_j e^{i\varphi_j} = \beta_j + i\alpha_j. \quad (4)$$

We rotate the Hamiltonians into an isospin basis $\Psi_{j'}$ under transformation $H_{j'} = U^\dagger_{jj'} H_j U_{jj'}$ where

$$U_{jj'} = \frac{1}{\sqrt{2}}\mathbb{1} \otimes \begin{pmatrix} e^{-i\varphi_j} & 1 \\ -1 & e^{i\varphi_j} \end{pmatrix} \quad (5)$$

and obtain a diagonal $H_{\mathrm{N}'}$ and block-diagonal $H_{\mathrm{S}'}$ as

$$H_{\mathrm{N}'} = \tau_z \otimes (E_p \mathbb{1} - \gamma_{\mathrm{N}} p\sigma_z), \quad (6)$$

$$H_{\mathrm{S}'} = \tau_z \otimes (E_p \mathbb{1} - \gamma_{\mathrm{S}} p\sigma_z) - \Delta\tau_x \otimes \mathbb{1}. \quad (7)$$

The spectra of $H_{\mathrm{N}'}$ and $H_{\mathrm{S}'}$ show particle and hole bands, denoted by $\tau = \pm$. Each band has two isospin branches denoted by $\sigma = \pm$. At a given energy E, there are eight corresponding eigen wave functions for $H_{\mathrm{N}'}$ and the other eight for $H_{\mathrm{S}'}$, denoted as

$$\chi^{\tau,\sigma}_{\mathrm{N}'} e^{i(\pm p^\tau_\sigma + \sigma\gamma_{\mathrm{N}})x} \quad \text{and} \quad \chi^{\tau,\sigma}_{\mathrm{S}'} e^{i(\pm k^\tau_\sigma + \sigma\gamma_{\mathrm{S}})x}, \quad (8)$$

respectively, where

$$p^\tau_\sigma = \sqrt{2m\,(\mu' - m\delta\gamma^2 + \tau E)}, \quad (9)$$

$$k^\tau_\sigma = \sqrt{2m\left(\mu' + m\delta\gamma^2 + \tau\sqrt{E^2-\Delta^2}\right)}, \quad (10)$$

with

$$\mu' = \mu + \tfrac{m(\gamma^2_{\mathrm{N}}+\gamma^2_{\mathrm{S}})}{4} \quad \text{and} \quad \delta\gamma^2 = \tfrac{\gamma^2_{\mathrm{S}}-\gamma^2_{\mathrm{N}}}{4}. \quad (11)$$

The particle-hole band and isospin states have representations as $\chi^{\tau,\sigma}_{\mathrm{N}'} = \begin{pmatrix} \delta_{\tau+}\delta_{\sigma+} & \delta_{\tau+}\delta_{\sigma-} & \delta_{\tau-}\delta_{\sigma+} & \delta_{\tau-}\delta_{\sigma-} \end{pmatrix}^T$ and $\chi^{\tau,\sigma}_{\mathrm{S}'} = u\begin{pmatrix} \delta_{\tau+}\delta_{\sigma+} & \delta_{\tau+}\delta_{\sigma-} & \delta_{\tau-}\delta_{\sigma+} & \delta_{\tau-}\delta_{\sigma-} \end{pmatrix}^T + v\begin{pmatrix} \delta_{\tau-}\delta_{\sigma+} & \delta_{\tau-}\delta_{\sigma-} & \delta_{\tau+}\delta_{\sigma+} & \delta_{\tau+}\delta_{\sigma-} \end{pmatrix}^T$, where $u^2 = 1 - v^2 = \frac{1}{2}\left(1 + \frac{\sqrt{E^2-\Delta^2}}{E}\right)$ and δ is the delta function. Below we drop $\hbar$ in all equations for convenience and take μ' and $\sqrt{2m\mu'}$ to be natural energy and momentum units, respectively (so $\gamma^2_{\mathrm{S}} + \gamma^2_{\mathrm{N}}$ causes no qualitative change but energy rescaling). Note that we consider energy range in which the hole excitations have real momenta [81].

In a BTK treatment, the interface is phenomenologically modeled by Hamiltonian $H_{\mathrm{I}}\delta(x)$, which generally has the same 4×4 representation as the bulk Hamiltonian. The matrix components reflect the interfacial properties as well as the physical discontinuity between both sides and specify transport processes through the interface. The original BTK model adopts one parameter $Z_0\tau_z \otimes \mathbb{1}$ to describe barrier effects from an oxide layer or local disorder [58]. For ferromagnet–superconductor heterostructures, H_{I} can be modeled as a Zeeman form $\mathbb{1} \otimes Z_h\,(\hat{n}\cdot\vec{\sigma})$ with unit direction $\hat{n} = (\sin\theta\cos\phi, \sin\theta\sin\phi, \cos\theta)$, which accounts for various spin-active processes such as spin-flip scattering, spin-dependent phase shift, and spin-related Andreev reflection [61–74]. In our case, we expect that the discontinuity of the bulk SOC and the interfacial SOC itself would play an active role in the transport. This effect is modeled by Rashba $Z_\alpha\tau_z \otimes \sigma_y$ and Dresselhaus $Z_\beta\tau_z \otimes \sigma_x$ components. To capture the most general interplay with spins, we incorporate all the factors above and write down our spin-orbit-active interface,

$$H_{\mathrm{I}} = \tau_z \otimes (Z_0\mathbb{1} + Z_\alpha\sigma_y + Z_\beta\sigma_x) + \mathbb{1} \otimes Z_h\,(\hat{n}\cdot\vec{\sigma}) \quad (12)$$

The two SOCs can be combined as $Z_\beta + iZ_\alpha = Z_\gamma e^{i\varphi_{\mathrm{I}}}$. In general, the spin basis of H_{I} and H_{N} can differ by another Euler rotation

$$U_{\mathrm{NI}} = \left(\mathbb{1} \otimes e^{-i\sigma_z\eta^{(3)}_{\mathrm{NI}}} e^{-i\sigma_y\eta^{(2)}_{\mathrm{NI}}} e^{-i\sigma_z\eta^{(1)}_{\mathrm{NI}}}\right). \quad (13)$$

We write the rotated $H_{\rm I}$ in a suggestive form as

$$U_{\rm NI}H_{\rm I}U_{\rm NI}^{\dagger} \equiv \begin{pmatrix} Z_0-Z_1 & Z_2e^{-i\zeta} & 0 & 0 \\ Z_2e^{i\zeta} & Z_0+Z_1 & 0 & 0 \\ 0 & 0 & -Z_0-Z_3 & -Z_4e^{-i(\zeta+\zeta')} \\ 0 & 0 & -Z_4e^{i(\zeta+\zeta')} & -Z_0+Z_3 \end{pmatrix}. \tag{14}$$

There are relations $Z_1^2+Z_2^2+Z_3^2+Z_4^2 = Z_h^2+Z_\gamma^2$ and $Z_1^2+Z_2^2-Z_3^2-Z_4^2 = 2Z_\gamma Z_h \sin\theta\cos(\phi-\varphi_{\rm I})$ that are independent of the Euler angles. Comparing Eq. (12) and Eq. (14), one can see that the three Euler angles effectively generate one additional variable.

In brief, the key ingredients on our system, the bulk SOCs $\alpha_j\sigma_y$ and $\beta_j\sigma_x$ as well as the interfacial parameters $Z_\alpha\sigma_y$, $Z_\beta\sigma_x$, and $Z_h\hat{n}\cdot\vec{\sigma}$, can be characterized by different vectors in spin space in the corresponding regions, as illustrated in Fig. 1. Below we study the system's transport properties as a function of these vectors.

III. BTK CALCULATIONS

Here we apply the BTK treatment to compute current-voltage relations of the system. Considering an incoming wave

$$\Psi_{\rm in}^{\tau,\sigma} = \chi_{\rm N'}^{\tau,\sigma}e^{i(\tau p_\sigma^\tau x+\sigma\gamma_{\rm N})}, \tag{15}$$

with energy E on the N side that propagates toward the interface (positive group velocity) and scatters through, we incorporate all possible outgoing waves and write down the wave functions on the N and S sides, as

$$\Psi_{\rm L} = U_{\rm NN'}\Big[\Psi_{\rm in}^{\tau,\sigma} + \sum\nolimits_\sigma e^{i\sigma\gamma_{\rm N}} \times\Big(b_\sigma\chi_{\rm N'}^{+,\sigma}e^{-ip_\sigma^+x} + a_\sigma\chi_{\rm N'}^{-,\sigma}e^{ip_\sigma^-x}\Big)\Big], \tag{16}$$

$$\Psi_{\rm R} = U_{\rm NS}U_{\rm SS'}\sum\nolimits_\sigma e^{i\sigma\gamma_{\rm S}} \times\Big(c_\sigma\chi_{\rm S'}^{+,\sigma}e^{ik_\sigma^+x} + d_\sigma\chi_{\rm S'}^{-,\sigma}e^{-ik_\sigma^-x}\Big), \tag{17}$$

respectively (all wave functions are represented in the real spin basis of $H_{\rm N}$). Because reflections (transmissions) should have the group velocity direction opposite to (same as) the incoming wave, only eight states are considered (see insets in Fig. 1). For an incoming electron ($\tau=+$), the amplitudes b, a, c, and d correspond to normal reflection, Andreev reflection [82], quasi-particle transmission and quasi-hole transmission, respectively, while for an incoming hole ($-$), a and b reverse their roles. The subscript σ of the amplitudes describes in-branch (cross-branch) processes if its sign is the same as (opposite to) the incoming wave. These amplitudes can be determined by two boundary conditions at the interface. The first one is the continuity of the wavefunction

$$\Psi_{\rm L}(0) = \Psi_{\rm R}(0), \tag{18}$$

while the second one can be obtained by integrating the BdG equation over an infinitesimal interval across the interface,

$$\int_{0^-}^{0^+}\Big\{\frac{1}{2}\big[H_{\rm N}\theta(-x)+U_{\rm NS}H_{\rm S}U_{\rm NS}^{\dagger}\theta(x)+{\rm H.c.}\big] +U_{\rm NI}H_{\rm I}U_{\rm NI}^{\dagger}\delta(x)\Big\}\Psi dx = 0, \tag{19}$$

where $\theta(x)$ is the step function and $\Psi(0^\pm) = \Psi_{\rm R/L}(0)$. We carefully keep the Hamiltonian Hermitian when it is expressed using the step function [83].

The probability current J is calculated from its definition $\partial_t\Psi^\dagger\Psi = -\partial_x J$. For each incoming wave $\Psi_{\rm in}^{\tau,\sigma}$, we calculate J corresponding to different scattering processes normalized by the incoming current and obtain combined currents carried by the in- and cross-branch normal (Andreev) reflections together, $J_{\tau,\sigma}^{\rm NR}$ ($J_{\tau,\sigma}^{\rm AR}$), as well as those carried by all the transmissions together, $J_{\tau,\sigma}^{\rm T}$ ($=1-J_{\tau,\sigma}^{\rm NR}-J_{\tau,\sigma}^{\rm AR}$ due to the probability conservation). Following the standard BTK treatment, the net charge current I induced by a voltage drop V across the junction can be evaluated as

$$I = \sum\nolimits_{\tau,\sigma} Ae\tau\int_0^\infty dE\Big\{\big(1-J_{\tau,\sigma}^{\rm NR}\big)\Big[f(E-\tau eV)-f(E)\Big] +J_{\tau,\sigma}^{\rm AR}\Big[f(E)-f(E+\tau eV)\Big]\Big\}, \tag{20}$$

where A is a constant associated with density of states, Fermi velocity, as well as an effective cross-sectional area, and $f(E) = [\exp({\rm E}/{\rm k_B T})+1]^{-1}$ is the Fermi distribution function at temperature T. We compute the I-V relation and normalized differential conductance (NDC) G/G_0, where $G = \frac{dI}{dV}$ and $G_0 = \frac{dI(\Delta=0)}{dV}$ is a reference value when the S side is normal.

IV. RESULTS

We first find that $\sum_\sigma J_{\tau,\sigma}^{\rm NR/AR/T}$ and hence $I(V)$ are independent of the Euler angles $\eta_{\rm NS}^{(i)}$. Therefore, parameters such as $\varphi_{\rm N}$ and $\varphi_{\rm S}$ that rely on the relative spin coordinate (RSC) between both sides should play no role on the transport either. We numerically confirm this independence by varying the ratio of Rashba and Dresselhaus SOC on each side. For the interface, $I(V)$ is independent of $\eta_{\rm NI}^{(i)}$ if one of Z_h and Z_γ in Eq. (12) is zero, so $\hat{n}$ or $\varphi_{\rm I}$ has no effect given $Z_\gamma=0$ or $Z_h=0$, respectively. We find that the scattering amplitude and probability current for each channel sensitively vary with RSC, but they compensate in the summation for $I(V)$. This implies that RSC may affect $I(V)$ as a result of interference in a multichannel or multiterminal system [73, 74] and also open interesting possibilities for spintronics.

In Fig. 2(a) we plot zero-bias NDC in the Z_0-Z_γ plane for a purely spin-orbit-active interface ($Z_h=0$). We see

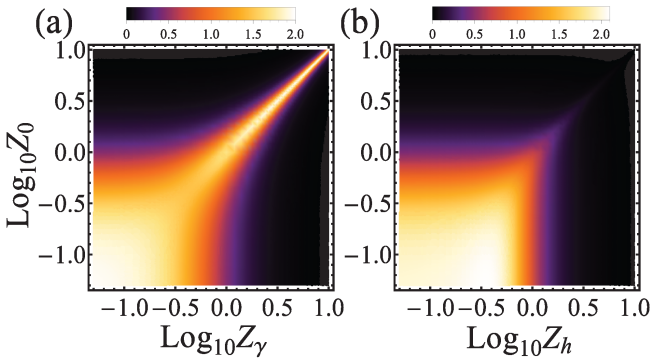

FIG. 2. (Color online) (a) [(b)] Zero-bias NDC (scaled by colors in bar graph) in the Z_0-Z_γ (Z_h) plane given Z_h (Z_γ) = 0. Data are for $\Delta = 0.002$, $\delta\gamma^2 = 0$, and $T = 0$.

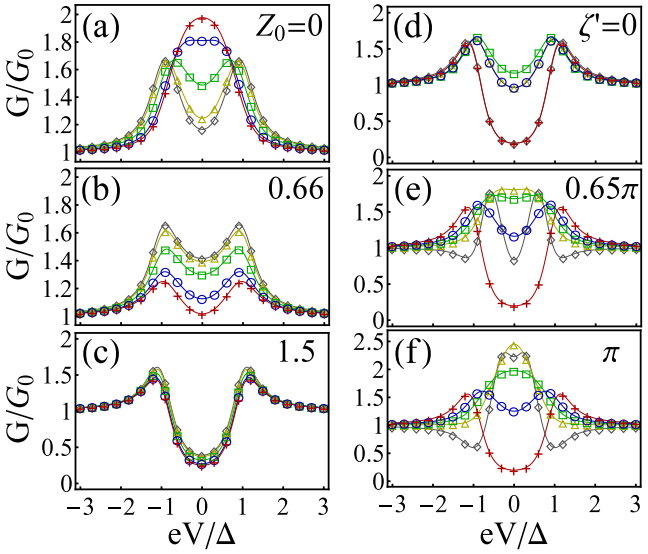

FIG. 3. (Color online) (a)–(c) Interfacial phase effects on NDC for a general spin-orbit-active interface described by Eq. (14) with $Z_0 = 0$, 0.66, and 1.5, respectively. Curves with diamonds, triangles, squares, circles, and crosses correspond to $\zeta' = 0$, 0.25π, 0.5π, 0.75π, and π, respectively. The other relevant parameters are set as $Z_1 = Z_3 = 0$, $Z_2 = Z_4 = 0.5$, $\Delta = 0.002$, $\delta\gamma^2 = 0$, and $T = 0.15\Delta$. (d)–(f) Charge imbalance effects on NDC at cases of $\zeta' = 0$, 0.65π, and π, respectively. Curves with diamonds, triangles, squares, circles, and crosses correspond to $m\delta\gamma^2 = -0.975$, -0.5, 0, 0.5, and 0.975, respectively. The other parameters are the same as (a)–(c) except $Z_0 = 0$ and $\delta\gamma^2$ varies.

that NDC reaches a high value when Z_γ is close to Z_0 and exhibits a symmetry under the exchange between Z_0 and Z_γ. To explain this, one can Euler rotate $H_{\rm I}$ to its eigenspin basis. The eigenvalues can be regarded as a set of characteristic barrier strengths $|Z_0 \pm Z_\gamma|$ that determine the BTK results. Such set is invariant under $Z_0 \leftrightarrow Z_\gamma$ and hence leads to the symmetry. To understand the NDC peaks, one can look at the scattering of the eigenspin states. At $Z_\gamma = Z_0$, electrons of one spin direction and holes of the opposite both see a clean interface $|Z_0 - Z_\gamma| = 0$, which maximizes the Andreev current as well as NDC. In other words, the presence of interfacial SOC can effectively lower the original BTK barrier ($|Z_0 - Z_\gamma| < Z_0$) [84]. In Fig. 2(b) we plot NDC in the Z_0-Z_h plane for a purely spin-active interface $Z_\gamma = 0$ for comparison. We see that there is no symmetry under $Z_0 \leftrightarrow Z_h$ and no conductance peak along the $Z_0 = Z_h$ line. Such differences illustrate the interfacial SOC effects that the original spin-active picture does not capture.

With the coexistence of Zeeman and SOC effects at the interface, the Euler angles $\eta^{(i)}_{\rm NI}$ are no longer irrelevant. We consider the general Hamiltonian of Eq. (14) and find that $I(V)$ is independent of ζ. The relevant variables are the five strength parameters $Z_{0,1,2,3,4}$ and the phase difference ζ' between off-diagonal elements of the particle and hole blocks. Notice that the role of ζ' is special: (1) it comes from the interplay between Z_h and Z_γ and (2) it does not alter the eigenvalues of the interfacial Hamiltonian. Therefore, its effects on the transport can be attributed to the interference between particle and hole channels. In Figs. 3(a)–3(c), we plot NDC vs V at various ζ' and Z_0 (we set $Z_1 = Z_3 = 0$ and $Z_2 = Z_4 = 0.5$ for illustrating the salient features from the interplay between ζ' and Z_0). At $Z_0 = 0$ (a), the curves are all above 1 and show a qualitative change from center-dent to center-peak types as ζ' goes through 0 (diamonds), 0.25π (triangles), 0.5π (squares), 0.75π (circles), and π (crosses). In this half period, the zero-bias NDC monotonically increases with ζ'. From $\zeta' = \pi$ to $\zeta' = 2\pi$, the deformation of curves completes the other half period and reverses back to the $\zeta' = 0$ case. As Z_0 increases, the center-peak curves drastically deform toward the center-dent type, and the trend of zero-bias NDC vs ζ' also reverses. At $Z_0 = 0.66$ (b), the $\zeta' = \pi$ curve has the lowest zero-bias NDC ≈ 1. At $Z_0 = 1.5$ (c), the center-dent curves remain and are well below 1 at low bias due to the suppression of transmissions and Andreev reflections (tunneling limit in the BTK model). The role of ζ' is not significant in this case. We turn to show one way to independently tune ζ' via the tuning of parameters in Eq. (12). Assuming the same spin basis on the N side and the interface ($\eta^{(i)}_{\rm NI} = 0$) and the interfacial Zeeman components tuned as $\theta = \pi/2$, $Z_h \cos\phi = Z_\gamma \sin^2\varphi_{\rm I}/\cos\varphi_{\rm I}$, and $Z_h \sin\phi = -Z_\gamma \sin\varphi_{\rm I}$, we obtain $Z_1 = Z_3 = 0$, $Z_2 = Z_4 = Z_\gamma/\cos\varphi_{\rm I}$, and $\zeta' = -2\varphi_{\rm I}$ by equating Eqs. (12) and (14). In this case, ζ' is associated with the ratio of Rashba and Dresselhaus components at the interface with properly controlled Zeeman components.

All the results above are for cases of balanced charge carriers between N and S sides ($\gamma_{\rm N} = \gamma_{\rm S}$). In Figs. 3(d)–3(f) we explore the effects of nonuniform SOC induced imbalance ($\delta\gamma^2 \neq 0$ resulting in Fermi momentum mismatch) and its interplay with the interfacial parameters. At $\zeta' = 0$, the curves are all of the center-dent type

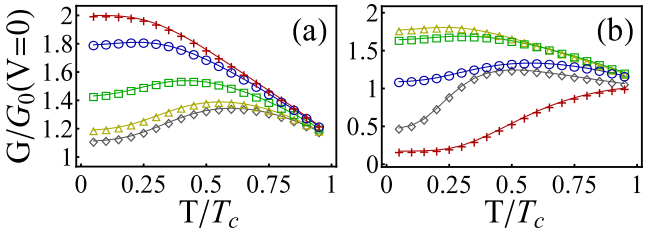

FIG. 4. (Color online) (a) Zero-bias NDC vs T at various ζ' [convention and setting are the same as Fig. 3(a)]. (b) Zero-bias NDC vs T at various $\delta\gamma^2$ [same as Fig. 3(e)].

and roughly display symmetry between positive and negative imbalance. The zero-bias NDC is far below 1 in the highly imbalanced cases. As ζ' increases, the $\delta\gamma^2 \leq 0$ curves deform more drastically than the $\delta\gamma^2 > 0$ ones. At $\zeta' = 0.65\pi$, the $m\delta\gamma^2 = -0.5$ curve develops a plateau around $V = 0$, indicating an incipience of a center peak. The $m\delta\gamma^2 = -0.975$ curve develops minimums around $eV = \Delta$. At $\zeta' = \pi$, the $m\delta\gamma^2 = -0.5$ and 0 curves show a center-peak structure, and the double minimums of the $m\delta\gamma^2 = -0.975$ curves become more significant. The range of zero-bias NDC as a function of $\delta\gamma^2$ also maximizes. These rich behaviors can be attributed to the high mismatch between the quasi-particle momenta on both sides and the interfacial phase difference ζ' between particle and hole channels, which together alter the scattering amplitudes in the BTK calculations.

Finally we discuss the temperature dependence of the transport. In Fig. 4 we plot zero-bias NDC vs T/T_c (T_c is the superconducting transition temperature) at various ζ' [(a), same convention and setting as Fig. 3(a)] or $\delta\gamma^2$ [(b), same as Fig. 3(e)]. The curves can exhibit three types of behavior: (1) monotonic increase, (2) monotonic decrease, and (3) first increase and then decrease (a reentrant phenomenon). These rich behaviors come from the same reason as the case of NDC vs V do, because high-energy excitations play a more important role at higher temperature. As a result, the conductance as a function of temperature is also sensitive to the bulk SOC and spin-orbit-active interface.

V. CONCLUSION

In conclusion, a general framework for superconducting heterostructures with SOC is developed and analyzed by generalizing the BTK scheme. Study of the conductance reveals the crucial role spin-orbit-active interface and nonuniform SOC play in determining the transport properties. In addition to being directly relevant for underpinning the physics of a range of hybrid systems of relevance to various fields including topological matter and spintronics, our work opens up many future research avenues. One is to apply and extend our transport analysis to other heterostructures, for example, to study the interplay with magnetic fields or ferromagnetism and also to study the multichannel interference effects in quasi-one-dimensional, higher-dimensional or multiterminal setups [73, 74, 85], also taking into account effects of fluctuations when a low-dimensional superconductor [86] is involved. Another is to analyze the impact on pairing symmetry, such as the possibility of p-wave pairing [87] and its consequences, and to establish a general framework also using complementary approaches such as quasiclassic formalism [88]. Finally, another important direction is to explore the consequences of nonuniformity and boundary/interface behaviors of SOC in ultracold atoms [89] by leveraging their tunability and amenability for probing the dynamics.

Acknowledgements: This work is supported by University of Cincinnati.

[1] Y. K. Kato, R. C. Myers, A. C. Gossard, and D. D. Awschalom, Observation of the Spin Hall Effect in Semiconductors, Science, **306**, 5703 (2004).
[2] C. L. Kane and E. J. Mele, Z_2 Topological Order and the Quantum Spin Hall Effect, Phys. Rev. Lett. **95**, 146802 (2005).
[3] B. A. Bernevig, T. L. Hughes and S.-C. Zhang, Quantum Spin Hall Effect and Topological Phase Transition in HgTe Quantum Wells, Science **314**, 5806 (2006).
[4] M. König, S. Wiedmann, C. Brüne, A. Roth, H. Buhmann, L. W. Molenkamp, X.-L. Qi, and S.-C. Zhang, Quantum Spin Hall Insulator State in HgTe Quantum Wells, Science **318**, 5851 (2007).
[5] J. Wang, X.-C. Ma, Y. Qi, Y.-S. Fu, S.-H. Ji, L. Lu, X. C. Xie, J.-F. Jia, X. Chen, and Q.-K. Xue, An unusual magnetoresistance effect in the heterojunction structure of an ultrathin single-crystal Pb film on silicon substrate, Nanotechnology **19**, 475708 (2009).
[6] I. Fischer, N. Shah, and A. Rosch, Crystalline phases in chiral ferromagnets: Destabilization of helical order, Phys. Rev. B **77**, 024415 (2008).
[7] S. Mülbauer, B. Binz, F. Jonietz, C. Pfleiderer, A. Rosch, A. Neubauer, R. Georgii, and P. Böni, Skyrmion Lattice in a Chiral Magnet, Science **323**, 915 (2009).
[8] M. Lee, W. Kang, Y. Onose, Y. Tokura, and N. P. Ong, Unusual Hall Effect Anomaly in MnSi Under Pressure, Phys. Rev. Lett. **102**, 186601 (2009).
[9] A. Hamann, D. Lamago, Th. Wolf, H. v. Löhneysen, and D. Reznik, Magnetic Blue Phase in the Chiral Itinerant Magnet MnSi, Phys. Rev. Lett. **107**, 037207 (2011).
[10] F. Krüger, U. Karahasanovic, and A. G. Green, Quantum Order-by-Disorder Near Criticality and the Secret of Partial Order in MnSi, Phys. Rev. Lett. **108**, 067003 (2012).
[11] S. Nadj-Perge, S. M. Frolov, E. P. A. M. Bakkers, and L. P. Kouwenhoven, Spin–orbit qubit in a semiconductor nanowire, Nature (London) **468**, 1084 (2010).
[12] C. Kloeffel, M. Trif, and D. Loss, Strong spin-orbit interaction and helical hole states in Ge/Si nanowires, Phys. Rev. B **84**, 195314 (2011).

[13] S. Nadj-Perge, V. S. Pribiag, J. W. G. van den Berg, K. Zuo, S. R. Plissard, E. P. A. M. Bakkers, S. M. Frolov, and L. P. Kouwenhoven, Spectroscopy of Spin-Orbit Quantum Bits in Indium Antimonide Nanowires, Phys. Rev. Lett. **108**, 166801 (2012).

[14] K. V. Shanavas and S. Satpathy, Electric Field Tuning of the Rashba Effect in the Polar Perovskite Structures, Phys. Rev. Lett. **112**, 086802 (2014).

[15] F. A. Zwanenburg, A. S. Dzurak, A. Morello, M. Y. Simmons, L. C. L. Hollenberg, G. Klimeck, S. Rogge, S. N. Coppersmith, and M. A. Eriksson, Silicon quantum electronics, Rev. Mod. Phys. **85**, 961 (2013).

[16] I. Žutić, Jaroslav Fabian, and S. Das Sarma, Spintronics: Fundamentals and applications, Rev. Mod. Phys. **76**, 323 (2004).

[17] M. Z. Hasan and C. L. Kane, Colloquium: Topological insulators, Rev. Mod. Phys. **82**, 3045 (2010).

[18] X.-L. Qi and S.-C. Zhang, Topological insulators and superconductors, Rev. Mod. Phys. **83**, 1057 (2011).

[19] L. Fu and C. L. Kane, Superconducting Proximity Effect and Majorana Fermions at the Surface of a Topological Insulator, Phys. Rev. Lett. **100**, 096407 (2008).

[20] R. M. Lutchyn, J. D. Sau, and S. Das Sarma, Majorana Fermions and a Topological Phase Transition in Semiconductor-Superconductor Heterostructures, Phys. Rev. Lett. **105**, 077001 (2010).

[21] Y. Oreg, G. Refael, and F. von Oppen, Helical Liquids and Majorana Bound States in Quantum Wires, Phys. Rev. Lett. **105**, 177002 (2010).

[22] A. Cook and M. Franz, Majorana fermions in a topological-insulator nanowire proximity-coupled to an s-wave superconductor, Phys. Rev. B **84**, 201105(R) (2011).

[23] V. Mourik, K. Zuo, S. M. Frolov, S. R. Plissard, E. P. A. M. Bakkers, and L. P. Kouwenhoven, Signatures of Majorana Fermions in Hybrid Superconductor-Semiconductor Nanowire Devices, Science **336**, 1003 (2012).

[24] M. Duckheim and P. W. Brouwer, Andreev reflection from noncentrosymmetric superconductors and Majorana bound-state generation in half-metallic ferromagnets, Phys. Rev. B **83**, 054513 (2011).

[25] S. B. Chung, H.-J. Zhang, X.-L. Qi, and S.-C. Zhang, Topological superconducting phase and Majorana fermions in half-metal/superconductor heterostructures, Phys. Rev. B **84**, 060510(R) (2011).

[26] S. Nadj-Perge, I. K. Drozdov, B. A. Bernevig, and A. Yazdani, Proposal for realizing Majorana fermions in chains of magnetic atoms on a superconductor, Phys. Rev. B **88**, 020407(R) (2013).

[27] S. Nadj-Perge, I. K. Drozdov, J. Li, H. Chen, S. Jeon, J. Seo, A. H. MacDonald, B. A. Bernevig, and A. Yazdani, Observation of Majorana fermions in ferromagnetic atomic chains on a superconductor, Science **346**, 602 (2014).

[28] H.-Y. Hui, P. M. R. Brydon, J. D. Sau, S. Tewari, and S. Das Sarma, Majorana fermions in ferromagnetic chains on the surface of bulk spin-orbit coupled s-wave superconductors, Sci. Rep. **5**, 8880 (2015).

[29] A. Yu Kitaev, Unpaired Majorana fermions in quantum wires, Phys. Usp. **44**, 131 (2001).

[30] C. J. Bolech and E. Demler, Observing Majorana bound States in p-Wave Superconductors Using Noise Measurements in Tunneling Experiments, Phys. Rev. Lett. **98**, 237002 (2007).

[31] F. Wilczek, Majorana returns, Nat. Phys. **5**, 614 (2009).

[32] M. Franz, Viewpoint: Race for Majorana fermions, Physics **3**, 24 (2010).

[33] E. M. Stoudenmire, J. Alicea, O. A. Starykh, and M. P. A. Fisher, Interaction effects in topological superconducting wires supporting Majorana fermions, Phys. Rev. B **84**, 014503 (2011).

[34] J. Alicea, Majorana fermions in a tunable semiconductor device, Phys. Rev. B **81**, 125318 (2010); New directions in the pursuit of Majorana fermions in solid state systems, Rep. Prog. Phys. **75**, 076501 (2012).

[35] C. W. J. Beenakker, Search for Majorana Fermions in Superconductors, Annu. Rev. Condens. Matter Phys. **4**, 113 (2013).

[36] K. T. Law, P. A. Lee, and T. K. Ng, Majorana Fermion Induced Resonant Andreev Reflection, Phys. Rev. Lett. **103**, 237001 (2009).

[37] C. Qu, Y. Zhang, Li Mao, and C. Zhang, Signature of Majorana Fermions in Charge Transport in Semiconductor Nanowires, arXiv:1109.4108.

[38] M. T. Deng, C. Yu, G. Huang, M. Larsson, P. Caroff, and H. Q. Xu, Anomalous Zero-Bias Conductance Peak in a Nb-InSb Nanowire-Nb Hybrid Device, Nano Lett. **12**, 6414 (2012).

[39] J. Liu, A. C. Potter, K. T. Law, and P. A. Lee, Zero-Bias Peaks in the Tunneling Conductance of Spin-Orbit-Coupled Superconducting Wires With and Without Majorana End-States, Phys. Rev. Lett. **109**, 267002 (2012).

[40] L. P. Rokhinson, X. Lui, and J. K. Furdyna, The fractional a.c. Josephson effect in a semiconductor-superconductor nanowire as a signature of Majorana particles, Nat. Phys. **8**, 795 (2012).

[41] A. Das, Y. Ronen, Y. Most, Y. Oreg, M. Heiblum, and H. Shtrikman, Zero-bias peaks and splitting in an Al-InAs nanowire topological superconductor as a signature of Majorana fermions, Nat. Phys. **8**, 887 (2012).

[42] C.-H. Lin, J. D. Sau, and S. Das Sarma, Zero-bias conductance peak in Majorana wires made of semiconductor/superconductor hybrid structures, Phys. Rev. B **86**, 224511 (2012).

[43] D. Roy, C. J. Bolech, and N. Shah, Majorana fermions in a topological superconducting wire out of equilibrium: Exact microscopic transport analysis of a p-wave open chain coupled to normal leads, Phys. Rev. B **86**, 094503 (2012); Nature of the zero-bias conductance peak associated with Majorana bound states in topological phases of semiconductor-superconductor hybrid structures, arXiv:1303.7036.

[44] A. D. K. Finck, D. J. Van Harlingen, P. K. Mohseni, K. Jung, and X. Li, Anomalous Modulation of a Zero-Bias Peak in a Hybrid Nanowire-Superconductor Device, Phys. Rev. Lett. **110**, 126406 (2013).

[45] H. O. H. Churchill, V. Fatemi, K. Grove-Rasmussen, M. T. Deng, P. Caroff, H. Q. Xu, and C. M. Marcus, Superconductor-nanowire devices from tunneling to the multichannel regime: Zero-bias oscillations and magnetoconductance crossover, Phys. Rev. B **87**, 241401(R) (2013).

[46] Ph. Jacquod and M. Büttiker, Signatures of Majorana fermions in hybrid normal-superconducting rings, Phys. Rev. B **88**, 241409(R) (2013).

[47] B. H. Wu, W. Yi, J. C. Cao, and G.-C. Guo, Noncollinear Andreev reflections in semiconductor nanowires, Phys. Rev. B **90**, 205435 (2014).

[48] J. Wang, M. Singh, M. Tian, N. Kumar, B. Liu, C. Shi, J. K. Jain, N. Samarth, T. E. Mallouk, and M. H. W. Chan, Interplay between superconductivity and ferromagnetism in crystalline nanowires, Nat. Phys. **6**, 389 (2010).

[49] S. Abay, D. Persson, H. Nilsson, F. Wu, H. Q. Xu, M. Fogelström, V. Shumeiko, and P. Delsing, Charge transport in InAs nanowire Josephson junctions, Phys. Rev. B **89**, 214508 (2014).

[50] Y. A. Bychkov and E. I. Rashba, Oscillatory effects and the magnetic susceptibility of carriers in inversion layers, J. Phys. C **17**, 6039 (1984).

[51] G. Dresselhaus, Spin-Orbit Coupling Effects in Zinc Blende Structures, Phys. Rev. **100**, 580 (1955).

[52] The interface could be a thin insulating layer, a layer with disorder, or simply a boundary between N and S regions (which could be a narrow region with rapidly changing physical properties).

[53] T. Ojanen, Topological π Josephson junction in superconducting Rashba wires, Phys. Rev. B **87**, 100506(R) (2013).

[54] J. Klinovaja and D. Loss, Fermionic and Majorana Bound States in Hybrid Nanowires with Non-Uniform Spin-Orbit Interaction, Eur. Phys. J. B **88**, 62 (2015).

[55] L. P. Gor'kov and E. I. Rashba, Superconducting 2D System with Lifted Spin Degeneracy: Mixed Singlet-Triplet State, Phys. Rev. Lett. **87**, 037004 (2001).

[56] V. M. Edelstein, Triplet superconductivity and magnetoelectric effect near the s-wave-superconductor–normal-metal interface caused by local breaking of mirror symmetry, Phys. Rev. B **67**, 020505(R) (2003).

[57] J. Linder and T. Yokoyama, Spin Current in Generic Hybrid Structures Due to Interfacial Spin-Orbit Scattering, Phys. Rev. Lett. **106**, 237201 (2011).

[58] G. E. Blonder, M. Tinkham, and T. M. Klapwijk, Transition from metallic to tunneling regimes in superconducting microconstrictions: Excess current, charge imbalance, and supercurrent conversion, Phys. Rev. B **25**, 4515 (1982).

[59] A. I. Buzdin, Proximity effects in superconductor-ferromagnet heterostructures, Rev. Mod. Phys. **77**, 935 (2005).

[60] F. S. Bergeret, A. F. Volkov, and K. B. Efetov, Odd triplet superconductivity and related phenomena in superconductor-ferromagnet structures, Rev. Mod. Phys. **77**, 1321 (2005).

[61] K. Xia, P. J. Kelly, G. E. W. Bauer, and I. Turek, Spin-Dependent Transparency of Ferromagnet/Superconductor Interfaces, Phys. Rev. Lett. **89**, 166603 (2002).

[62] E. Zhao, Tomas Löfwander, and J. A. Sauls, Nonequilibrium superconductivity near spin-active interfaces, Phys. Rev. B **70**, 134510 (2004).

[63] A. Cottet and W. Belzig, Superconducting proximity effect in a diffusive ferromagnet with spin-active interfaces, Phys. Rev. B **72**, 180503 (2005).

[64] C.-Te Wu, O. T. Valls, and K. Halterman, Tunneling conductance and spin transport in clean ferromagnet/ferromagnet/superconductor heterostructures, Phys. Rev. B **90** 054523 (2014).

[65] O. Shevtsov and T. Löfwander, Spin imbalance in hybrid superconducting structures with spin-active interfaces, Phys. Rev. B **90**, 085432 (2014).

[66] A. Millis, D. Rainer, and J. A. Sauls, Quasiclassical theory of superconductivity near magnetically active interfaces, Phys. Rev. B **38**, 4504 (1988).

[67] T. Tokuyasu, J. A. Sauls, and D. Rainer, Proximity effect of a ferromagnetic insulator in contact with a superconductor, Phys. Rev. B **38**, 8823 (1988).

[68] M. Fogelström, Josephson currents through spin-active interfaces, Phys. Rev. B **62**, 11812 (2000).

[69] V. V. Ryazanov, V. A. Oboznov, A. Yu. Rusanov, A. V. Veretennikov, A. A. Golubov, and J. Aarts, Coupling of Two Superconductors through a Ferromagnet: Evidence for a π Junction, Phys. Rev. Lett. **86**, 2427 (2001).

[70] M. J. M. de Jong and C. W. J. Beenakker, Andreev Reflection in Ferromagnet-Superconductor Junctions, Phys. Rev. Lett. **74**, 1657 (1995).

[71] M. S. Kalenkov and A. D. Zaikin, Crossed Andreev reflection at spin-active interfaces, Phys. Rev. B **76**, 224506 (2007).

[72] F. Hübler, M. J. Wolf, T. Scherer, D. Wang, D. Beckmann, and H. v. Löneysen, Observation of Andreev Bound States at Spin-active Interfaces, Phys. Rev. Lett. **109**, 087004 (2012).

[73] M. Colci, K. Sun, N. Shah, S. Vishveshwara, and D. J. Van Harlingen, Anomalous polarization-dependent transport in nanoscale double-barrier superconductor/ferromagnet/superconductor junctions, Phys. Rev. B **85**, 180512(R) (2012).

[74] K. Sun, N. Shah, and S. Vishveshwara, Transport in multiterminal superconductor/ferromagnet junctions having spin-dependent interfaces, Phys. Rev. B **87**, 054509 (2013).

[75] K. Maki, *Superconductivity*, edited by R. D. Parks (Marcel-Dekker, New York, 1969), Vol. 2, Ch. 18.

[76] R. Meservey and P. M. Tedrow, Spin-polarized electron tunneling, Phys. Rep. **238**, 173 (1994).

[77] A. V. Lopatin, N. Shah, and V. M. Vinokur, Fluctuation Conductivity of Thin Films and Nanowires Near a Parallel-Field-Tuned Superconducting Quantum Phase Transition, Phys. Rev. Lett. **94**, 037003 (2005).

[78] A. Rogachev, A. T. Bollinger, and A. Bezryadin, Influence of High Magnetic Fields on the Superconducting Transition of One-Dimensional Nb and MoGe Nanowires,Phys. Rev. Lett. **94**, 017004 (2005).

[79] N. Shah and A. Lopatin, Microscopic analysis of the superconducting quantum critical point: Finite-temperature crossovers in transport near a pair-breaking quantum phase transition, Phys. Rev. B **76**, 094511 (2007).

[80] A. Del Maestro, B. Rosenow, N. Shah, and S. Sachdev, Universal thermal and electrical transport near the superconductor-metal quantum phase transition in nanowires, Phys. Rev. B **77**, 180501(R) (2008).

[81] In the high imbalance limit $\delta\gamma^2 \to \pm 1$, the hole excitations have imaginary momenta in a wide range of E and thus become ill-defined in the BdG scenario.

[82] A. F. Andreev, The Thermal Conductivity of the Intermediate State in Superconductors, Sov. Phys. JETP **19**, 1228 (1964).

[83] For example, the discontinuity of SOC between N and S sides should not be described by linear momentum terms simply as $p\theta(x)$ but a Hermitian form $\frac{1}{2}[p\theta(x) + \text{h.c.}]$.

[84] Note that along the line $Z_0 = Z_\gamma$, the minimum of NDC appears at a middle point due to a non-monotonic relative behavior between G and G_0.

[85] N. Shah and A. Rosch, Nonequilibrium conductance of a three-terminal quantum dot in the Kondo regime: Per-

turbative renormalization group study, Phys. Rev. B **73**, 081309(R) (2006).

[86] M. Sahu, M.-H. Bae, A. Rogachev, D. Pekker, T.-C. Wei, N. Shah, P. M. Goldbart, and A. Bezryadin, Individual topological tunneling events of a quantum field probed through their macroscopic consequences, Nat. Phys. **5**, 503 (2009). J. D. Sau, B. I. Halperin, K. Flensberg, and S. Das Sarma, Number conserving theory for topologically protected degeneracy in one-dimensional fermions, Phys. Rev. B **84**, 144509 (2011). L. Fidkowski, R. M. Lutchyn, C. Nayak, and M. P. A. Fisher, Majorana zero modes in one-dimensional quantum wires without long-ranged superconducting order, Phys. Rev. B **84**, 195436 (2011). M. W. Brenner, S. Gopalakrishnan, J. Ku, Timothy J. McArdle, J. N. Eckstein, N. Shah, P. M. Goldbart, and A. Bezryadin, Cratered Lorentzian response of driven microwave superconducting nanowire-bridged resonators: Oscillatory and magnetic-field induced stochastic states, Phys. Rev. B **83**, 184503 (2011). M. W. Brenner, D. Roy, N. Shah, and A. Bezryadin, Dynamics of superconducting nanowires shunted with an external resistor, Phys. Rev. B **85**, 224507 (2012).

[87] A. F. Volkov, F. S. Bergeret, and K. B. Efetov, Odd Triplet Superconductivity in Superconductor-Ferromagnet Multilayered Structures, Phys. Rev. Lett. **90**, 117006 (2003). C. J. Bolech and T. Giamarchi, Point-Contact Tunneling Involving Low-Dimensional Spin-Triplet Superconductors, Phys. Rev. Lett. **92**, 127001 (2004); Keldysh study of point-contact tunneling between superconductors, Phys. Rev. B **71**, 024517 (2005); Tunnelling in organic superconductors, J. Low Temp. Phys. **142**, 221 (2006). R. S. Keizer, S. T. B. Goennenwein, T. M. Klapwijk, G. Miao, G. Xiao and A. Gupta, A spin triplet supercurrent through the half-metallic ferromagnet CrO2, Nature (London) **439**, 825 (2006). M. Eschrig and T. Lofwander, Triplet supercurrents in clean and disordered half-metallic ferromagnets, Nat. Phys. **4**, 138 (2008). J. Linder, T. Yokoyama, A. Sudbo and M. Eschrig, Pairing Symmetry Conversion by Spin-Active Interfaces in Magnetic Normal-Metal-Superconductor Junctions, Phys. Rev. Lett. **102**, 107008 (2009). B. Almog, S. Hacohen-Gourgy, A. Tsukernik, and G. Deutscher, Triplet order parameter component at Co/CoO/In contacts, Phys. Rev. B **84**, 054514 (2011). P. V. Leksin, N. N. Garif'yanov, I. A. Garifullin, Ya. V. Fominov, J. Schumann, Y. Krupskaya, V. Kataev, O. G. Schmidt, and B. Büchner, Evidence for Triplet Superconductivity in a Superconductor-Ferromagnet Spin Valve, Phys. Rev. Lett. **109**, 057005 (2012). Y. Tanaka, M. Sato, and N. Nagaosa, Symmetry and Topology in Superconductors – Odd-Frequency Pairing and Edge States, J. Phys. Soc. Jpn. **81**, 011013 (2012). F. S. Bergeret and I. V. Tokatly, Singlet-Triplet Conversion and the Long-Range Proximity Effect in Superconductor-Ferromagnet Structures with Generic Spin Dependent Fields, Phys. Rev. Lett. **110**, 117003 (2013). P. Gentile, M. Cuoco, A. Romano, C. Noce, D. Manske, and P. M. R. Brydon, Spin-Orbital Coupling in a Triplet Superconductor-Ferromagnet Junction, Phys. Rev. Lett. **111**, 097003 (2013). K. Sun, C.-K. Chiu, H.-H. Hung, and J. Wu, Tuning between singlet, triplet, and mixed pairing states in an extended Hubbard chain, Phys. Rev. B **89**, 104519 (2014). X. Liu, J. D. Sau, and S. Das Sarma, Universal spin-triplet superconducting correlations of Majorana fermions, arXiv:1501.07273.

[88] E. A. Demler, G. B. Arnold, and M. R. Beasley, Superconducting proximity effects in magnetic metals, Phys. Rev. B **55**, 15174 (1997). V. Stanev and V. Galitski, Quasiclassical Eilenberger theory of the topological proximity effect in a superconducting nanowire, Phys. Rev. B **89**, 174521 (2014). M. Alidoust and K. Halterman, Long-range spin-triplet correlations and edge spin currents in diffusive spin-orbit coupled SNS hybrids with a single spin-active interface, arXiv:1502.05719.

[89] Y.-J. Lin, K. Jiménez-García and I. B. Spielman, Spin-orbit-coupled Bose-Einstein condensates, Nature (London) **471**, 83 (2011). X.-J. Liu, L. Jiang, H. Pu, and H. Hu, Probing Majorana fermions in spin-orbit-coupled atomic Fermi gases, Phys. Rev. A **85**, 021603(R) (2012). P. Wang, Z.-Q. Yu, Z. Fu, J. Miao, L. Huang, S. Chai, H. Zhai, and J. Zhang, Spin-Orbit Coupled Degenerate Fermi Gases, Phys. Rev. Lett. **109**, 095301 (2012). L. W. Cheuk, A. T. Sommer, Z. Hadzibabic, T. Yefsah, W. S. Bakr, and M. W. Zwierlein, Spin-Injection Spectroscopy of a Spin-Orbit Coupled Fermi Gas, Phys. Rev. Lett. **109**, 095302 (2012). C. Qu, Z. Zheng, M. Gong, Y. Xu, Li Mao, X. Zou, G. Guo, and C Zhang, Topological superfluids with finite-momentum pairing and Majorana fermions, Nat. Commun. **4**, 2710 (2013). W. Zhang and W. Yi, Topological Fulde-Ferrell-LarkinOvchinnikov states in spin–orbit-coupled Fermi gases, Nat. Commun. **4**, 2711 (2013). C. Chen, Inhomogeneous Topological Superfluidity in One-Dimensional Spin-Orbit-Coupled Fermi Gases, Phys. Rev. Lett. **111**, 235302 (2013). K. Sun, C. Qu, C Zhang, Spin–orbital angular momentum coupled Bose-Einstein condensates, arXiv:1411.1737. C. Qu, K. Sun, C Zhang, Quantum phases of Bose-Einstein condensates with synthetic spin–orbital angular momentum coupling, arXiv:1502.08052.